Direct and *in situ* growth of 1T' MoS_2 and 1T $MoSe_2$ on electrochemically synthesized MXene as an electrocatalyst for hydrogen generation

Sin-Yi Pang[‡1], *Weng-Fu Io*[‡1], *Lok-Wing Wong*[1], *Jiong Zhao*[1] *and Jianhua Hao*[1]*

[‡]S.Y Pang and W.F. Io contributed equally to this work.

[1] Department of Applied Physics, The Hong Kong Polytechnic University, Hung Hom, Hong Kong, P.R. China

*Corresponding author: jh.hao@polyu.edu.hk

Highlight

- 1T'-MoS_2 and 1T-$MoSe_2$ were directly grown on electrochemically synthesized fluoride-free MXene.
- Extendable strategy for the direct and *in situ* growth of phase-controlled TMDs on the MXene substrates.
- In acidic solution, the engineered catalyst exhibits high catalytic activity of 167 mV at current density of 10 mA cm^{-2}.

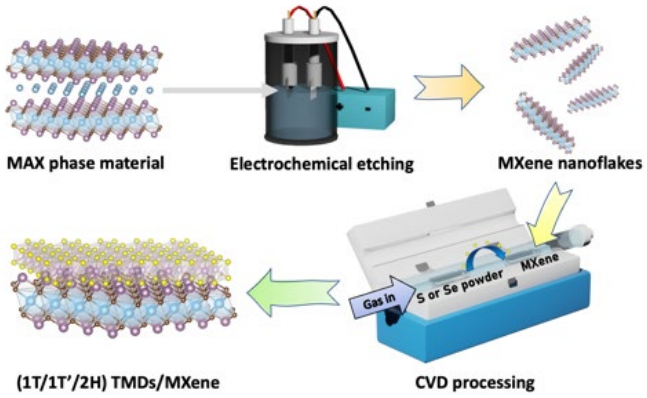

Abstract

Crystal phase modulations in two-dimensional (2D) materials have garnered extensive interest because of their intriguing features and potential applications. Nonetheless,

synthesizing some specific phases of metastable transition metal dichalcogenides (TMDs) remains a challenge due to the restricted selectivity under chemical and physical treatments, especially for direct growth of specific phase of TMDs on 2D substrates to form heterostructures. Taking the merits of MXene with tunable atomic vacancies and surface chemistry via surface functionalization, the phase of epitaxially grown TMDs on 2D MXene can be significantly affected. In this work, 1T'-MoS_2 and 1T-$MoSe_2$ were directly grown on electrochemically synthesized MXene under controlled oxidization conditions and selected MXene substrate. Owing to the synergistic effect of TMDs and MXene, the TMDs/MXene heterostructure catalysts exhibit good electrochemical activity under acidic conditions, with a low overpotential of 167 mV at a current density of 10 mA cm^{-2}. Our work not only demonstrates the distinct chemical characteristic of various MXenes feasible for surface engineering which promotes the direct and *in situ* growth of phase controlled TMDs on MXene substrates but also displays the high electrochemical activity in TMDs/MXene heterostructure catalysts.

Keywords: Catalyst, Electrochemical etching, Direct growth, HF-free MXene, 1T $MoSe_2$, 1T' MoS_2

1 Introduction

Two-dimensional (2D) materials have piqued the interest of researchers and turned the discipline into a dynamic and fascinating research topic upon the discovery of novel physical properties in graphene[1-4]. Crystal phase control is essential for adjusting the inherent physicochemical properties of 2D materials tailed to meet the demands of their diverse applications in electronics, optoelectronics, and electrocatalysis[5]. However, the challenge in direct growth with selected phase synthesis and stabilizing phase limits the synthesis of robust metallic phase of group VI transition metal dichalcogenides (TMDs)[6], and the metastable TMDs coupled with different materials is greatly coveted as an uncharted territory. To date, several strategies for phase control in the polymorphic TMDs have been developed, including alkali metal intercalation, flux method, hydrothermal reaction, and colloidal synthesis[7, 8], as well as physical treatments such as electron beam irradiation, plasma hot electron transfer,

mechanical strain, and flux method[6, 9-11]. Unfortunately, the synthesis of metastable phases such as octahedral phase and its distorted phases (1T and 1T') is more complex because of their various chemical compositions[12, 13]. Differing from the semiconducting phase such as 2H phase of MoS_2 and $MoSe_2$, it is encouraging that the semi-metallic 1T- and 1T'-MoS_2 and $MoSe_2$ have shown to possess high electrocatalytically active towards hydrogen evolution reaction (HER)[7, 14].

Noted that the selection of substrate greatly influences the epitaxial growth of 2D materials or nanoparticles. Substrate engineering allows the phase engineering of nanoparticles[13] (PEN) or an epitaxial layer by employing different substrates. For example, the growth orientation of Pt nanoparticles can be regulated *via* a mismatch in the lattice between the target growth material and the MXene substrate.[15] MXene is an important class of 2D materials with a wide range of applications due to its unique and adjustable physicochemical properties, while its applications span from electrocatalysts and biosensors to superconductors[16-18]. They are typically produced by selectively etching the "A" layer of the MAX phase material[19]. The layered MAX phase material is defined in the generic formulation $M_{n+1}AX_n$ hexagonal carbides and nitrides, where n ranges from 1 to 4, M is an early transition metal, A is commonly a group 13 or 14 element, such as Al, Ga, Si, or Ge, and X is carbon and/or nitrogen. MXene is sandwiched by the "A" layer on a regular basis. Various etchants have been applied including hydrofluoric acid (HF) etching, *in-situ* HF production by combining lithium fluoride/hydrochloric acid, alkali etching, Lewis molten salt etching, and electrochemical etching (E-etching)[18, 20-22]. Surface functionalization such as -O, -F, -Cl, -OH is then covalently linked with MXene during the selective etching of the monoatomic "A" layers, endowing MXene with remarkable hydrophilicity, high flexibility, and conductivity[19]. The etching conditions and post-treatments determine the flake size, synthesis yield, surface functionalization, and nature of MXenes[23]. For instance, the newly developed HF-etched double transition metal MXene Mo_2TiC_2 has shown unique properties with the generated Mo vacancies by post electrochemical treatment, which can anchor single Pt atom and function as an effective electrocatalyst [24]. In contrast to the HF-etched MXene, HF-free/E-etched MXene shows diverse physical and chemical characteristics , especially a larger lattice constant beneficial for the growth of PEN, which results from the atomic structure differences caused by different functionalized atoms[15, 17]. Additionally, the surface selenization strategy on HF-etched is also an effective method for improving the electrochemical properties of MXenes,

in which MXenes are converted to transition metal selenides with high capacity and outstanding structural stability while the inner layer of MXenes are intentionally preserved[25].

Herein, we present a systematic strategy for epitaxially synthesizing crystal phase-controlled 1T or 1T'-MoX_2 (X=S, Se) layers atop E-etched Mo_2TiC_2 MXene with controlled chemical vapor deposition (CVD) method. Through the E-etching and annealing processes, the Mo_2TiC_2 MXene develops surface point vacancies, allowing the formation of stable metallic 1T'-MoS_2 and 1T-$MoSe_2$ while only the semiconducting 2H-phase MoS_2 was grown on HF-etched Mo_2TiC_2 in pervious study[26]. The heterostructure TMDs/MXene catalysts exhibit good electrochemical activity in acidic solution attributing to the advantage of synergistic effect between TMDs and MXene, with a low overpotential of 167 mV at a current density of 10 mA cm^{-2}. Our work paves a new way for epitaxial growth of 2D materials on 2D HF-free MXene substrate and demonstrates the potential to be extended to PEN, hence providing a novel method to construct effective TMDs/MXene heterostructures for electrocatalysis and other device applications [27].

2 RESULT AND DISCUSSION

2.1 Fabrication and characterization of TMDs/MXene heterostructure

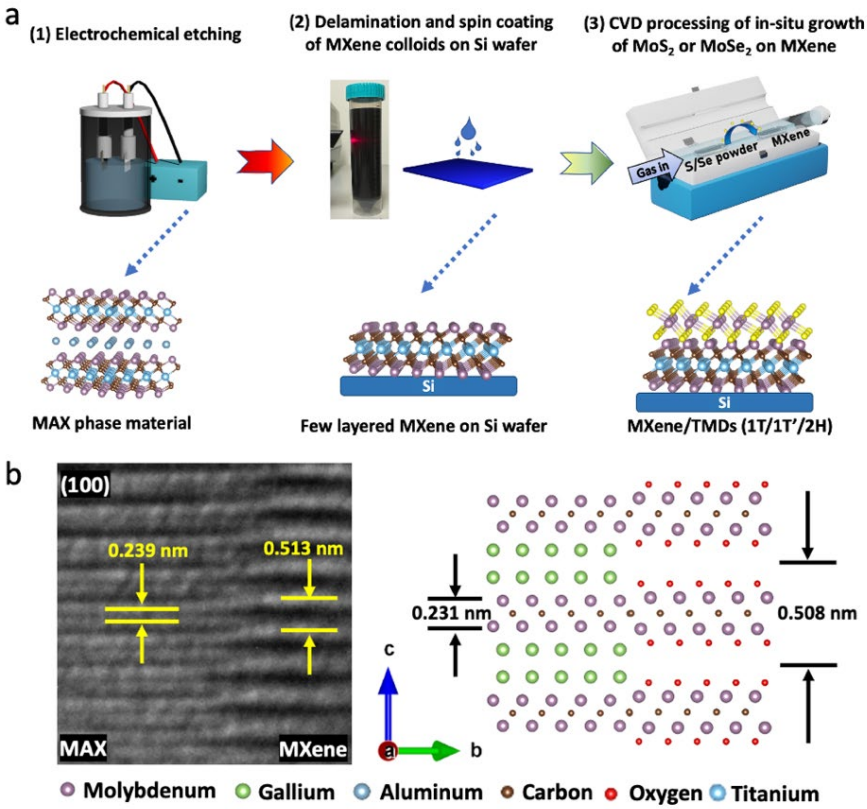

Figure 1. (a) Schematic of the process of *in situ* growth of MoS_2 or $MoSe_2$ on MXene. (b) The TEM image partially etched Mo_2Ga_2C.

Figure 1a illustrates a schematic of the synthesis process of TMDs epitaxially grown on MXene. First, high-quality HF-free MXene was synthesized by E-etching approach that promoted the selective removal of "A" layers from quaternary/trinary transition metal carbides (Detail in experimental section). Subsequently, the as-synthesized MXene was spin-coated on a silicon substrate and sulfurized through CVD at a temperature of 600 ºC. Cyclic voltammogram (CV) was used to determine the proper range of the etching voltages. **Figure S1** shows the CVs for various MAX phase materials with etching potentials varying from 0 to 1.8 V vs. RHE. The first anodic peak at 0.7 V was assigned to the "A" layer reacting to the acid which resulted in the removal of the "A" layer (Stage 1), whereas the second anodic peak at 1.2 V indicates that both the "M" and "A" layers react with the electrolyte, resulting in over-etching of MXene due to the destruction of the M-C bonding (Stage 2)[20]. To facilitate selective etching of the "A" layer, the MXene was etched at a mild heating temperature of 55 °C with a small bias of 0.7 V, leading to the dissolution of the aluminum or gallium layer wedged in MAX phase material in diluted HCl electrolyte in the form of aluminum chloride and gallium chloride.

Sonication was used to delaminate the as-synthesized material. The X-ray diffraction (XRD) and Raman patterns in **Figure S2-S3** show the removal of 'A' layer from the MAX phase by eliminating the 'A' layer vibration peak, and peak shift correlates to an increase in interlayer spacing. **Figure 1b** shows a cross-section of partially etched MAX-MXene interface imaged by transmission electron microscopy (TEM) along the *a*-axis at (100) face. The Mo_2C sandwiched by double Ga atoms in Mo_2Ga_2C has an atomic thickness of 0.231 nm in the density functional theory (DFT) computed lattice model, whereas the Mo_2CO_2 lattice has an atomic thickness of 0.508 nm. The lattice fringes of the TEM image match with the computed model. The Mo_2Ga_2C XRD results agree with the TEM picture in which a sharp peak shift from 9.89° to 9.6° caused by the removal of the Ga layer matched to an increase in interlayer separation for the stacked Mo_2C[28]. The smaller peak shift may attribute to the stacking of the Mo_2C MXene from the intercalant-free mechanical exfoliation, which minimizes the uncertainty raise from the intercalation. It also facilitates the direct comparison of using different MXenes or oxidation time.

The lattice configuration of the MXene nanosheet was captured using TEM, as shown in **Figure S4**. The imaged area was at the flake center, demonstrating that the Mo-based MXene holds a tightly packed hexagonal structure. For Mo_2TiC_2, the TEM imaged the near atomic layer of Ti atoms, thus a lighter contrast is observed[24]. The appearances of the lattice change at the edge and center positions of the nanoflake (**Figure S5**). This variation is resulted from surface group defects and strain[15] induced on the top and bottom surfaces, as well as the etching process. E-etching is an edge site-initiated etching process[29] analogous to the *in situ* HF etching, whereas the HF etching is a grain boundary etching process[30]. The concentration of etchant is proportional to the defect concentration. The etchant used in this reaction is mild when compared to traditional methods[31] and thus atomic point defects were found on the MXene instead of defect clusters[32]. The defects on the MXene are further demonstrated by the HAADF-STEM image of Mo_2TiC_2 and the associated line profile, as shown in Figure S5b. The associated accessible planes and defects provide an anchor location for chemically vaporized S ion[24] immobilization.

2.2 The effect of oxidation time and CVD growth temperature on Mo_2TiC_2

The MXene was first treated with 1 M KOH before CVD process for oxidizing the MXene and grafting oxo-functionalized on it[15]. The Raman spectroscopy was used to evaluate the oxidization effect of OH^- ions to MXene (**Figure S6a**). The Raman shifts at 312 and 690 cm^{-1} are attributable to the h-MoO_3 intermediate[33] after 0.5 hour of oxidation. When the oxidation time was increased to 1 hour, the Raman responses became stronger, with intense signals at 183 and 285 cm^{-1}. When the oxidation time was increased to 2 hours, the α-MoO_3 produced a succession of Raman signals at 250, 650, 862, and 912 cm^{-1} that are consistent with the literature[34]. A board peak at 160 cm^{-1} is attributed to the bulk MoO_3 and TiO_2 layers[35]. The surface of the MXene is covered by anatase to extremely oxidize it for 48 hours, and the Raman spectrum is comparable to that of oxidized titanium carbide[20]. As presented in the following equation, the MAX phase material electrode undergoes anodic polarization during the electrochemical etching process:

$$Mo_2TiAlC + yCl^- + (2x+z)H_2O \rightarrow Mo_2TiC(OH)_{2x}Cl_yO_z + Al^{3+} + (x + z)H_2 + (y + 3)e^-$$

The CVD processing is capable of removing the functional group produced during the E-etching process[15] and causing atomic defects on MXene since the Mo-O bonding is stronger than Mo-C bonding[24]. The removal of such functionalizes exposes the inner Ti layer to the surface[24]. To determine the optimal sulfurization temperature required for MoS_2 synthesis on MXene and postulate the surface termination change on MXene after CVD, identical oxidized Mo_2TiC_2 was sulfurized at different temperature (**Figure S6b**). The Raman spectra show that MXene has no reactivity to sulfur when the temperature is not higher than 500 °C. We propose that the peaks at 150, 197, 395 cm^{-1} are corresponding anatase to TiO_2 formed by surface oxidation in the interaction with the environment after the surface functional group removal[36] by comparing the MXene annealed at different temperatures and the oxidized MXene in the previous report[20]. The incorporation of the -o surface functional groups facilitate the formation of surface defects due to the surface functionalized removal in the annealing process[37].

2.3 The effects of sulfurization and selenization on various MXenes

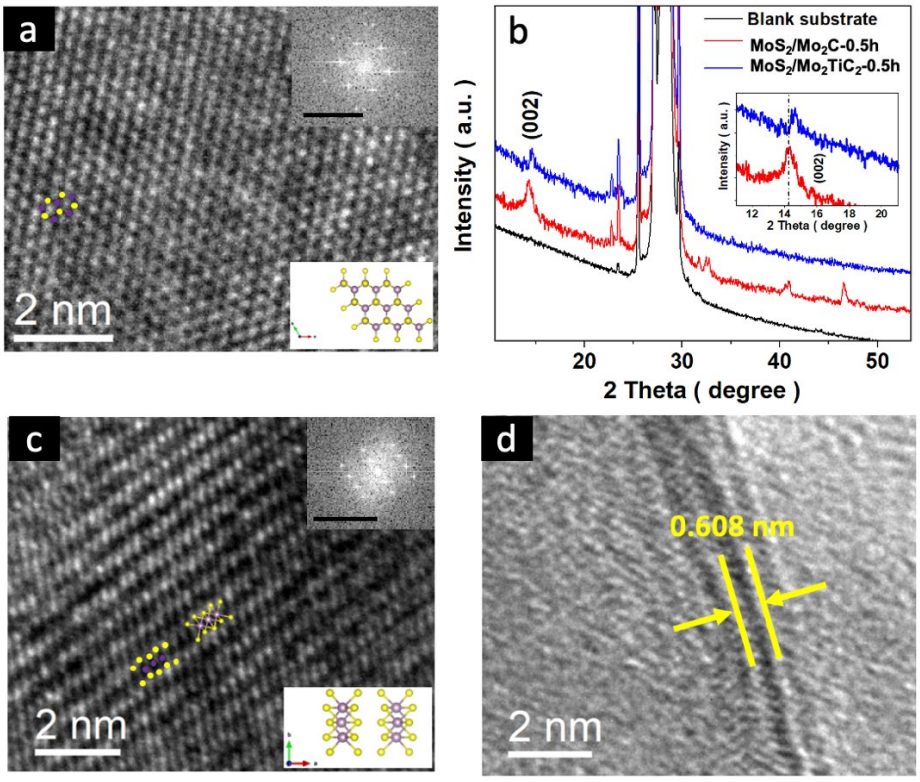

Figure 2. (a) The TEM image of MoS_2/Mo_2C-0.5h. (b) The XRD pattern of sulfurized MXenes. The (c) top and the (d) edge TEM images of the MoS_2/Mo_2TiC_2-0.5h sample. The scales for Fourier transform inset are 10 1/nm.

The phase of the sample were confirmed by the TEM picture and XRD pattern in **Figure 2a-b** for MoS_2/Mo_2C-0.5h, where the (002) peak for MoS_2/Mo_2C-0.5h sample at 14.1° is ascribed to the 2H MoS_2 [Ref. [13]]. As shown in **Figure S5**, atomic defects were produced on the Mo_2TiC_2 MXene as a result of the manufacturing method and annealing procedure, and a defect-rich substrate[31] is advantageous to the formation of 1T' phase MoS_2 for sliding sulfur atom and stabilizing the 1T' structure[31, 38]. The XRD pattern (**Figure 2b**), the crystalline ordering in the HRTEM image (**Figure 2c**) and the diagonal atomic-scale edge structure (**Figure 2d**) of the MoS_2/Mo_2TiC_2-0.5h sample indicate the 1T' octahedral lattice[39]. **Figure 3a** illustrates the Raman spectra derived from MoS_2/Mo_2TiC_2-0.5h, which show the archetypal J_1, J_2, and J_3 vibration modes for 1T' MoS_2. J_1 involves two modes of vibration, including the out-of-plane and in-plane shearing vibrations of each atom stripe for the other atoms in the chain. J_2 peak at 226 cm^{-1} owing to the relative motion of two zigzag chains, whereas J_3 is related to the off-axis vibration of tending to split each zigzag chain into two stripes[8, 40]. The formation of 1T' MoS_2 on the surface of the MXene was also suggested by the X-ray

photoelectron spectroscopy (XPS) results (**Figure S7**). Mo 3d and S 2s spectra could be fitted into three peaks at 226.5, 229.1, and 232.2 eV for defective MoS_2 and Mo-S bonding for Mo $3d_{5/2}$ and Mo $3d_{3/2}$, respectively. For the S2p spectra, three peaks may be fitted at 167.6, 164.3, and 162.4 eV for metal sulfate, S $2p_{1/2}$, and S $2p_{3/2}$. There is a modest shift in the spectrum when compared to the documented 1T MoS_2 in earlier studies[41, 42], indicating the presence of 1T MoS_2. Furthermore, the stability of heterostructure sample is tested by comparing the Raman spectra of the freshly synthesized sample to the sample exposed to air for half a year; the exact peak is visible in both curves, confirming the exceptional stability of the 1T' MoS_2 on MXene (**Figure S8**). Interestingly, the epitaxial growth of the MoS_2 on HF-free Mo_2TiC_2 (1T' phase) is different from the HF etched Mo_2TiC_2 sample (2H phase)[26], and it is rationally ascribed to the grafting of Mo-O terminal with a H atom from electrochemical etching process, resulting in the formation of a Mo-OH intermediate. Mo-C bonds are broken because of the stronger Mo-O bond in Mo-OH_2, resulting in the formation of a Mo-OH_2 leaving group[24] and more vacancy in HF free Mo_2TiC_2. Additionally, Raman responses of the out-of-plane ordered quaternary MXene $Mo_2Ti_2C_3$ derived MoS_2 have one more pair of peaks than the MoS_2/Mo_3C_2-0.5h sample as shown. The Raman peaks at 224 and 340 cm^{-1} may be ascribed to the TiS_2 vibration peaks[36], whereas the others are assigned to the MoS_2 vibration peaks. The difference between the growth of TMDs on $Mo_2Ti_2C_3$ and Mo_2TiC_2 may attribute to the higher stability in thicker MXene since increase of n (in $M_{n+1}X_n$) preserves the stacking configuration while enhancing its energetic preference, and thus it may affect the reaction step rate in the E-etching process and result in more explored inner layer[43].

The MoS_2 exhibits two primary Raman modes in the 2H phase of A_{1g} and E_{1g} modes[44] for the MoS_2/Mo_2C-0.5h samples, in good agreement with our control-MoS_2 samples grown with typical MoO_3 precursor (**Figure S9a**), previous XRD discussion and literature[31, 45]. The out-of-plane vibration mode attributes to the opposite vibration of two S atoms against the Mo atom, whereas the in-plane vibration of the Mo and S atoms vibrate against each other[8]. The effect of the oxidization time of the MXene on sulfurization is studied based on Raman spectra (**Figure S10**). When the oxidation duration was raised to 48 hours, the 2H MoS_2 signal decreased in MoS_2/Mo_2C sample, showing that the over-oxidized MXene is not favorable for growing MoS_2. Additionally, the Raman peak for the MXene is hardly discernible and it is attributed to the suppression of signal for the MXene substrate after the sulfurization process

due to the covering of MoS_2, as suggested in the electron energy loss spectroscopy (EELS) (**Figure S11**).

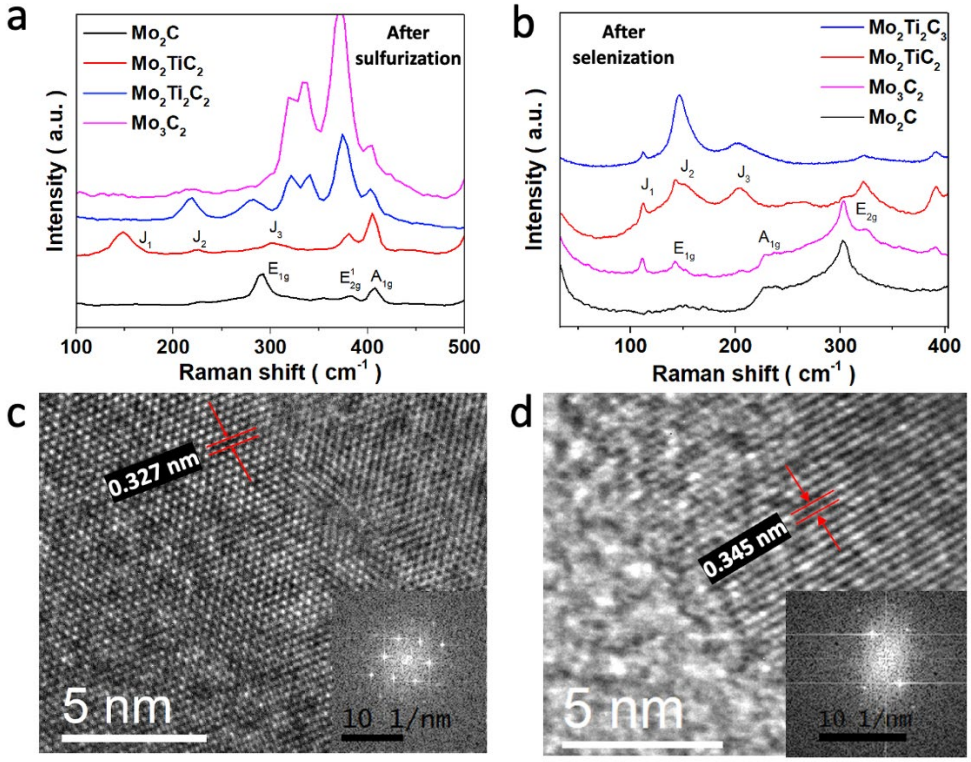

Figure 3. The Raman spectra for Mo_2C, Mo_3C_2, Mo_2TiC_2 and $Mo_2Ti_2C_3$ after (a) sulfurization and (b) selenization process and post-oxidization with KOH for 30 mins. (c) HRTEM image of 1T-$MoSe_2$ at the center of the flake (d) 1T-$TiSe_2$ at the edge of the $Mo_2Ti_2C_3$ flake. The inset is the FFT picture of the TEM images.

On the other hand, selenization of MXene was then carried out to validate the influence of the surface functional group defect on TMDs development. For mono element MXene, the Mo_3C_2 and Mo_2C shared a comparable set of Raman peaks at 142, 228, and 301 cm^{-1}, matching to the E_{1g}, A_{1g}, and E_{2g} vibration modes of 2H $MoSe_2$ (**Figure 3b**), which are also compatible with the $MoSe_2$ converted from MoO_3 (**Figure S9b**). The 111 (J_1), 146 (J_2), and 202 (J_3) are ascribed to 1T $MoSe_2$ (**Figure 3b**). The HRTEM and diffraction pattern from the FFT measurement indicated the single crystalline nature of $MoSe_2$ and $TiSe_2$ to determine the phase of the $MoSe_2/Mo_2Ti_2C_3$-0.5 h sample (**Figure 3c-d**). The hexagonal lattice of the TMDs is displayed in well-resolved 2D lattice fringes, as demonstrated in the literature[46]. Notably, 1T-$TiSe_2$ was discovered at the edge of the edge whereas 1T-$MoSe_2$ was found in the center of the flake. This is attributable to the H_2(10%)/Ar mix gas utilized in the selenization, which

causes more vacancy on the edge of the MXene due to the interaction between H_2 and -O functional group. The difference in the phase structure between the MoS_2/$MoSe_2$ on double element MXene substrates may be rationally explained as a difference in atomic size and lattice mismatch between the TMDs and MXene. According to our DTF calculation and previous literature[13], 1T'-MoS_2 and 1T'-$MoSe_2$ have lattice parameters of 0.311 and 0.325 nm, respectively, whereas Mo_2TiC_2 MXene has a lattice parameter of 0.292 nm. Since functionalized MXene may vary in lattice size[17], 1T'-MoS_2 has a comparable lattice parameter to MXene, but 1T'-$MoSe_2$ has a high lattice misfit to MXene and there is no space for the 1T'-$MoSe_2$ to achieve a more stable configuration by sliding the Se atom[13]. Moreover, Se has a larger atomic radius than S and Mo, the atomic surface of the MXene may be incapable of facilitating the growth of 1T' phase $MoSe_2$ when the atom size of the diffused atom is similar to the size of vacancy. As a result, the choice of MXene substrate influences the formation of TMDs due to the highly modifiable surface of MXene, and the TMDs development on MXene is tunable by employing suitable MXene.

2.4 The electrochemical properties of TMDs/MXene

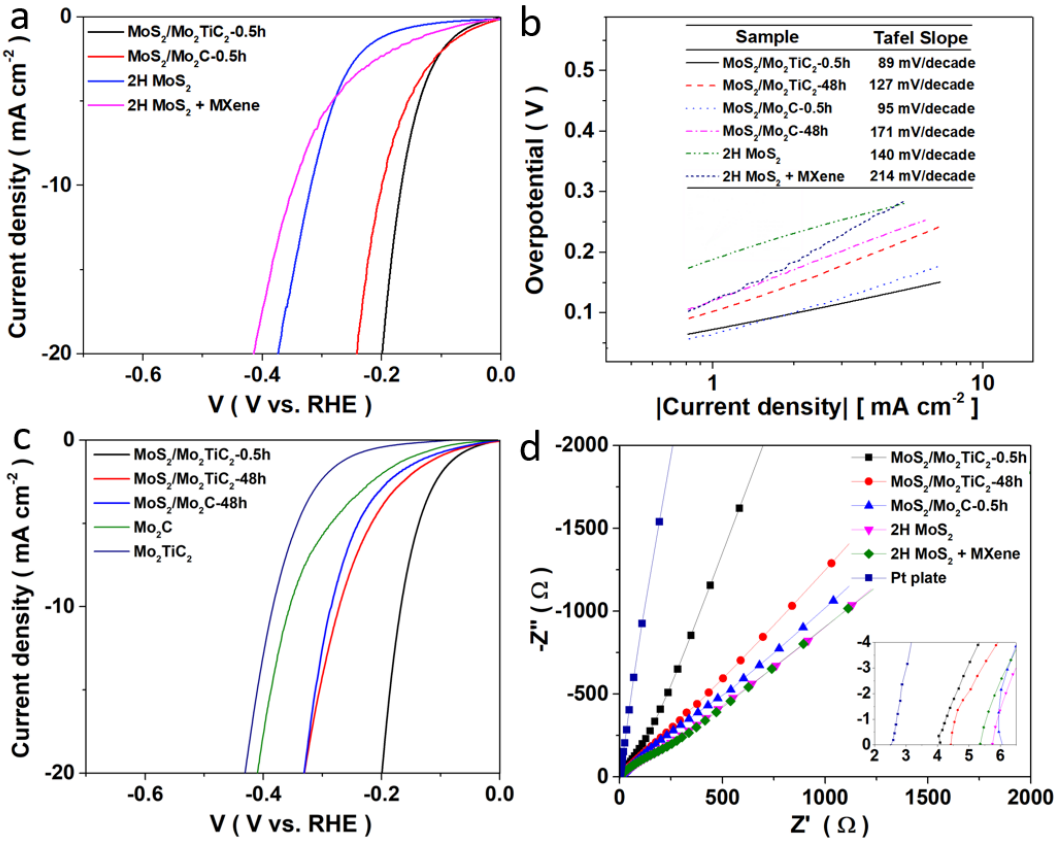

Figure 4. (a) The linear sweep voltammetry (LSV) and (b) and the corresponded Tafel slope of catalysts. (c) LSVs for the bare MXene and the MoS_2/MXene under different synthesis conditions. (d) Nyquist plots for comparison of the MoS_2/Mo_2TiC_2, MoS_2/Mo_2C samples. The inset shared the x-y axis with the Nyquist plots.

Phase control on the epitaxial growth of TMDs considerably affects the electrochemical activity of the TMDs/MXene as catalysts. As a proof-of-concept demonstration, the HER activity of heterostructure catalysts was examined in 0.5 M H_2SO_4 solution using a polished glassy carbon electrode with a graphite rod as the counter electrode. In acidic solution, the MoS_2/Mo_2TiC_2-0.5h sample performed a lower an overpotential of 167 mV (V *vs.* RHE) to achieve a specific current density of 10 mA cm^{-2} (**Figure 4a**) and a Tafel slope of 89 mV/decade (**Figure 4b**), indicating more rapid HER kinetics thorough Volmer-Tafel reaction path in comparison to MoS_2/Mo_2TiC_2-48h sample. This result shows that the *in situ* metallic 1T' phase MoS_2 facilitates the hydrogen evolution process by combining the gapless contact with the metallic MXene, and the phase engineering with aim of attaining 1T'-MoS_2 improved its HER activity. The overpotential of the MoS_2/Mo_2TiC_2-0.5h sample is only 167 mV to reach a current

density of 10 mA cm^{-2}, which is considerably lower than that of MoS_2/Mo_2TiC_2-48h (197 mV), MoS_2/Mo_2C-0.5h (271 mV), MoS_2/Mo_2C-48h (283 mV), 2H MoS_2 (310 mV) and 2H MoS_2 + MXene (347 mV) samples at a specific current density of 10 mA cm^{-2}, suggesting the excellent electrocatalytic efficiency of Mo_2TiC_2/MoS_2-0.5h catalyst. Furthermore, the bare MXenes in acidic solution exhibit only mediocre electrocatalytic activities towards HER with an overpotential of 385 mV and 356 mV at a specific current density of 10 mA cm^{-2} for Mo_2C and Mo_2TiC_2, respectively. Considering the comparable electrocatalytic behavior between Mo_2C and Mo_2TiC_2, the LSV curve difference between MoS_2/MXenes can be attributed to the epitaxial growth material over the MXene.

Consequently, the catalytic performance for HER of Mo_2TiC_2/MoS_2-0.5h sample is comparable to state-of-the-art metallic TMDs based catalyst[39] (**Table S1)**, where the catalyst demonstrates good catalytic activity without further doping or defect introduction used in reported MoS_2 catalysts. The MoS_2/Mo_2C-0.5h and MoS_2/Mo_2TiC_2-48h samples demonstrated a low electrocatalytic activity against HER and a high overpotential of 197 mV and 271 mV at a particular current density of 10 mA cm^{-2}, as shown in **Figure 4c**. Additionally, the less conducive to redox-active electrochemical reactions and inert S edge of the surface 2H MoS_2 are responsible for the large overpotential[10]. As a result, the control sample of 2H MoS_2 and the 2H MoS_2-MXene mixed sample show sluggish HER activity with high overpotentials of 310 mV and 347 mV at a particular current density of 10 mA cm^{-2}, respectively. We hypothesize that the slightly higher HER performance of MoS_2/Mo_2C-0.5h sample to the 2H MoS_2 samples is attributable to the distinct heterojunction of the unique chemical synthesis approach and the synergistic effect of MXene[45], and thus the TMDs/MXene heterostructure outperforms 2H MoS_2 and physically mixed 2H MoS_2 and MXene sample which owing high contact mismatch (**Figure 4a**).

To investigate the origin of the advanced electrochemical activity of the MoS_2/Mo_2TiC_2-0.5h sample amongst other heterostructure TMDs/MXene samples, electrochemical impedance spectroscopy (EIS) was implemented to evaluate the contact resistance for the samples (**Figure 4d**). The metallic heterostructure MoS_2/Mo_2TiC_2-0.5h exhibits a high conductivity with a low contact resistance in the system of 4.08 ohms with the conductive support of the MXene substrate, signifying the benefits of MoS_2/Mo_2TiC_2-0.5h sample with barrier-free quick kinetics, a low diffusion resistance and a strong ion transfer activity of the catalyst. Compared to the bare Mo_2TiC_2, the contact resistance of the MoS_2/Mo_2TiC_2-0.5h sample is greatly reduced by

1.75 ohms. Nevertheless, the other MoS_2-based catalysts have higher resistance to the system ranging from 5.36 to 7.69 ohms (**Table S2**) and display transmission line behavior, indicating relatively slow ion diffusion transfer activity.

The contact resistance of the MoS_2/Mo_2TiC_2-0.5h system is also comparable to the pure platinum metal plate (**Figure 4d**). The diffusion tail of the lower-frequency region in the Nyquist plot of MoS_2/Mo_2TiC_2-0.5h with a high slope suggests that the sample is less resistive than the other electrocatalysts[47]. It can be attributed to the combination of the semiconducting MXene and the metallic 1T' MoS_2, which turns the overall nature of the electrode material into semi-metallic. Moreover, we also measured the EIS for the bare MXenes to directly compare the electrochemical of the MXene before and after the sulfurization. The Nyquist plot suggests that electrode/electrolyte electron transfer resistance is reduced after the epitaxial growth of metallic MoS_2 on the surface of the MXene. Notably, the 1T'-MoS_2 growth on Mo_2TiC_2 (MoS_2/Mo_2TiC_2-0.5h sample) displayed Mo defects in the basal plane in the TEM image in the previous section as shown in **Figure 2c**, which can produce a novel electronic state to govern the hydrogen absorption behavior of the coordination S atom, hence improving intrinsic activity of whole heterostructure catalyst[39]. The results suggest that the *in situ* growth of MoS_2 on MXene heterostructure catalyst has greater catalytic activity than pristine MXene and MoS_2, demonstrating the synergetic effect of the engineered heterostructure. The heterostructure also affects the electron transfer kinetics and electrochemical activity. By utilizing the charge-transfer kinetics-favored design, the MoS_2/Mo_2TiC_2-0.5h catalyst demonstrates high kinetics in acidic electrolytes.

3 Conclusion

In conclusion, we present the direct and *in situ* growth of metallic phase TMDs (1T'-MoS_2 and 1T-$MoSe_2$) on various HF-free MXenes and the origins of the different phases are investigated through structural analysis. The unique property of E-etched $MoTi_2C$ with surface defects and an active site to capture S ions provides a favorable site for developing specific phase TMDs. The catalytic activity of the TMDs/MXene heterostructure catalysts is similar to that of the state-of-the-art catalyst in an acidic solution. Furthermore, the 1T'-MoS_2 on MoS_2/Mo_2TiC_2-0.5h sample is stable in air, demonstrating the protective effect of MXene on metastable 1T'-MoS_2. This study presents the importance of HF-free MXene on the direct growth of phase-controlled TMDs and opens an avenue for phase engineering of 2D materials

on double transition metal MXene coupling with diverse designs for various applications in electrochemical energy conversion.

4 Experimental section

Materials and reagents: Molybdenum aluminum carbide, Molybdenum titanium aluminum carbide and Molybdenum gallium carbide (200 mesh, 99 percent purity) were acquired from Laizhou Kai Ceramic material Co., Ltd. Sigma supplied the hydrochloride, potassium hydroxide, lithium fluoride, sulfuric acid, and sodium hydroxide. Aladdin-reagent Co., Ltd. provided polyvinyl alcohol (88%) for this experiment. All materials were utilized as received, with no further purification.

Synthesis of MXene: The molybdenum carbide and molybdenum titanium carbide were fabricated by the E-etching method. The CFCs for E-etching were purified as previously reported. The CFCs were cleaned with ethanol and acetone before being immersed in the HNO_3 solution for 6 hours under reflux. The NaOH solution neutralized the CFCs, which were then rinsed several times with water and dried in a 60 °C oven. The MAX phase material was mixed with carbon black in a 95:5 ratio and evenly drop-casted onto the CFC substrate. With a moderate heating temperature of 55 °C and an appropriate bias of 0.7 V, the A layer wedged in MAX phase material was dissolved in the dilute HCl electrolyte. The multi-layered MXene was sonicated and rinsed with a mixed solution of ethanol and deionized water to remove the un-etched residue MAX phase material. After filtering the remaining MAX phase material, 2D MXene was purified by collecting the supernatant produced after centrifugation at 3000 rpm for 5 minutes.

Oxidizing processing for MXenes: To aid in the epitaxial development of the TMDs, we further enhanced the oxo-functionalized-rich surface of the MXene. 1 mL of 1 M KOH was mixed with 1 mL of MXene with the concentration of 1 mg/mL. After 30 minutes, 1 hour, 2 hours, and 48 hours, the as-mixed solution was vortexed. The solution would be rinsed for numerous times with deionized water until the pH value of the solution reached natural.

CVD process: The oxidized MXene precursor was employed as the Mo source precursor on the Si substrate, and excess S/Se powder was used to provide a S/Se-rich environment for the in-situ CVD process. The precursors were placed at separate quartz boats and the S/Se source was placed in the upstream of the furnace. For the sulfurization process, the S powder

and oxidized MXene precursor were heated to 160°C and 600 °C, respectively, and the temperature was held for 1 hour at atmospheric pressure with Argon as the carrier gas flowing at 30 sccm. For the selenization process, the Se powder and oxidized MXene precursor were heated to 300 °C and 800 °C, respectively, and the temperature was held for 30 minutes at atmospheric pressure with 10% H_2/Ar mix gas flowing at 10 sccm. After the synthesis process, the CVD furnace was naturally cooled down to room temperature. The 2H MoS_2 and $MoSe_2$ were created by swapping out the MXene "seed" with a MoO_3 "seed."

DFT calculation for bandgap and lattice structure: The Quantum espresso software package[48] was used for all first-principles simulations based on density functional theory (DFT). The exchange and correlation energies were computed using a parameterized local-density approximation (DFT-PBE). The kinetic energy cutoff for the plane wave is 700 eV, and a vacuum layer of 15 Å is utilized. Only the x and y dimensions change for MXene cell optimization and relaxation (i.e. 2D xy constraint). The dipole and van der Waals (vdW) interactions were taken into account. A 12 × 12 x 1 Monkhorst k-point grid was utilized for MXenes.

CRediT authorship contribution statement

Sin-Yi Pang: Conceptualization, Methodology, Investigation, Writing – original draft, Writing – review & editing. **Weng-Fu Io:** Methodology, Investigation, Writing – review & editing. **Lok-Wing Wong:** Methodology, Writing – review & editing. **Jiong Zhao:** Methodology, Writing – review & editing. **Jianhua Hao:** Supervision, Funding acquisition, Project administration, Writing – review & editing.

Declaration of Competing Interest

The authors declare that they have no known competing financial interests or personal relationships that could have appeared to influence the work reported in this paper.

Acknowledgments

This work was fully supported by the grant from Research Grants Council of Hong Kong (GRF No. PolyU 15301020).

Reference

[1] Gogotsi, Y.; Anasori, B. The rise of MXenes. *ACS Nano* **2019**, *13*, 8491-8494.

[2] Wu, Z.;Lyu, Y.;Zhang, Y.;Ding, R.;Zheng, B.;Yang, Z.;Lau, S. P.;Chen, X. H.; Hao, J. Large-scale growth of few-layer two-dimensional black phosphorus. *Nature Materials* **2021**, *20*, 1203-1209.

[3] Ding, R.;Liu, C.-K.;Wu, Z.;Guo, F.;Pang, S.-Y.;Wong, L. W.;Io, W. F.;Yuan, S.;Wong, M.-C.; Jedrzejczyk, M. B. A general wet transferring approach for diffusion-facilitated space-confined grown perovskite single-crystalline optoelectronic thin films. *Nano letters* **2020**, *20*, 2747-2755.

[4] VahidMohammadi, A.;Rosen, J.; Gogotsi, Y. The world of two-dimensional carbides and nitrides (MXenes). *Science* **2021**, *372*, 1165.

[5] Io, W. F.;Yuan, S.;Pang, S. Y.;Wong, L. W.;Zhao, J.; Hao, J. Temperature-and thickness-dependence of robust out-of-plane ferroelectricity in CVD grown ultrathin van der Waals α-In_2Se_3 layers. *Nano Research* **2020**, *13*, 1897.

[6] Enyashin, A. N.;Yadgarov, L.;Houben, L.;Popov, I.;Weidenbach, M.;Tenne, R.;Bar-Sadan, M.; Seifert, G. New route for stabilization of 1T-WS2 and MoS2 phases. *The Journal of Physical Chemistry C* **2011**, *115*, 24586-24591.

[7] Yu, Y.;Nam, G.-H.;He, Q.;Wu, X.-J.;Zhang, K.;Yang, Z.;Chen, J.;Ma, Q.;Zhao, M.; Liu, Z. High phase-purity 1T'-MoS2-and 1T'-MoSe2-layered crystals. *Nature chemistry* **2018**, *10*, 638-643.

[8] Tan, S. J. R.;Sarkar, S.;Zhao, X.;Luo, X.;Luo, Y. Z.;Poh, S. M.;Abdelwahab, I.;Zhou, W.;Venkatesan, T.; Chen, W. Temperature-and phase-dependent phonon renormalization in 1T'-MoS2. *ACS nano* **2018**, *12*, 5051-5058.

[9] Qu, Y.;Medina, H.;Wang, S. W.;Wang, Y. C.;Chen, C. W.;Su, T. Y.;Manikandan, A.;Wang, K.;Shih, Y. C.; Chang, J. W. Wafer Scale Phase-Engineered 1T-and 2H-MoSe2/Mo Core–Shell 3D-Hierarchical Nanostructures toward Efficient Electrocatalytic Hydrogen Evolution Reaction. *Advanced Materials* **2016**, *28*, 9831-9838.

[10] Chang, K.;Hai, X.;Pang, H.;Zhang, H.;Shi, L.;Liu, G.;Liu, H.;Zhao, G.;Li, M.; Ye, J. Targeted Synthesis of 2H-and 1T-Phase MoS2 Monolayers for Catalytic Hydrogen Evolution. *Advanced Materials* **2016**, *28*, 10033-10041.

[11] Ambrosi, A.;Sofer, Z.; Pumera, M. 2H→ 1T phase transition and hydrogen evolution activity of MoS 2, MoSe 2, WS 2 and WSe 2 strongly depends on the MX 2 composition. *Chemical Communications* **2015**, *51*, 8450-8453.

[12] Duerloo, K.-A. N.;Li, Y.; Reed, E. J. Structural phase transitions in two-dimensional Mo-and W-dichalcogenide monolayers. *Nature communications* **2014**, *5*, 1-9.

[13] Lai, Z.;He, Q.;Tran, T. H.;Repaka, D.;Zhou, D.-D.;Sun, Y.;Xi, S.;Li, Y.;Chaturvedi, A.; Tan, C. Metastable 1T'-phase group VIB transition metal dichalcogenide crystals. *Nature Materials* **2021**, *20*, 1113-1120.

[14] Liu, L.;Wu, J.;Wu, L.;Ye, M.;Liu, X.;Wang, Q.;Hou, S.;Lu, P.;Sun, L.; Zheng, J. Phase-selective synthesis of 1T′ MoS2 monolayers and heterophase bilayers. *Nature materials* **2018**, *17*, 1108-1114.

[15] Pang, S. Y.;Io, W. F.; Hao, J. Facile atomic-level tuning of reactive metal-support interaction in Pt QDs@ HF-free MXene heterostructure for accelerating pH-universal hydrogen evolution reaction. *Advanced Science* **2021**, *8*.

[16] Song, M.;Pang, S. Y.;Guo, F.;Wong, M. C.; Hao, J. Fluoride-free 2D niobium carbide MXenes as stable and biocompatible nanoplatforms for electrochemical biosensors with ultrahigh sensitivity. *Advanced Science* **2020**, *7*, 2001546.

[17] Kamysbayev, V.;Filatov, A. S.;Hu, H.;Rui, X.;Lagunas, F.;Wang, D.;Klie, R. F.; Talapin, D. V. Covalent surface modifications and superconductivity of two-dimensional metal carbide MXenes. *Science* **2020**, *369*, 979-983.

[18] Hu, M.;Zhang, H.;Hu, T.;Fan, B.;Wang, X.; Li, Z. Emerging 2D MXenes for supercapacitors: status, challenges and prospects. *Chemical Society Reviews* **2020**, *49*, 6666-6693.

[19] Anasori, B.;Lukatskaya, M. R.; Gogotsi, Y. 2D metal carbides and nitrides (MXenes) for energy storage. *Nature Reviews Materials* **2017**, *2*, 16098.

[20] Pang, S.-Y.;Wong, Y.-T.;Yuan, S.;Liu, Y.;Tsang, M.-K.;Yang, Z.;Huang, H.;Wong, W.-T.; Hao, J. Universal Strategy for HF-Free Facile and Rapid Synthesis of Two-

dimensional MXenes as Multifunctional Energy Materials. *Journal of the American Chemical Society* **2019**, *141*, 9610-9616.

[21] Yuan, S.;Pang, S.-Y.; Hao, J. 2D transition metal dichalcogenides, carbides, nitrides, and their applications in supercapacitors and electrocatalytic hydrogen evolution reaction. *Applied Physics Reviews* **2020**, *7*, 021304.

[22] Li, Y.;Shao, H.;Lin, Z.;Lu, J.;Liu, L.;Duployer, B.;Persson, P. O.;Eklund, P.;Hultman, L.; Li, M. A general Lewis acidic etching route for preparing MXenes with enhanced electrochemical performance in non-aqueous electrolyte. *Nature Materials* **2020**, *19*, 894-899.

[23] Du, Z.;Wu, C.;Chen, Y.;Cao, Z.;Hu, R.;Zhang, Y.;Gu, J.;Cui, Y.;Chen, H.; Shi, Y. High-Entropy Atomic Layers of Transition-Metal Carbides (MXenes). *Advanced Materials* **2021**, *33*, 2101473.

[24] Zhang, J.;Zhao, Y.;Guo, X.;Chen, C.;Dong, C.-L.;Liu, R.-S.;Han, C.-P.;Li, Y.;Gogotsi, Y.; Wang, G. Single platinum atoms immobilized on an MXene as an efficient catalyst for the hydrogen evolution reaction. *Nature Catalysis* **2018**, *1*, 985-992.

[25] Sha, D.;Lu, C.;He, W.;Ding, J.;Zhang, H.;Bao, Z.;Cao, X.;Fan, J.;Dou, Y.; Pan, L. Surface selenization strategy for V_2CT_x MXene toward superior Zn-Ion storage. *ACS nano* **2022**, *16*, 2711-2720.

[26] Chen, C.;Xie, X.;Anasori, B.;Sarycheva, A.;Makaryan, T.;Zhao, M.;Urbankowski, P.;Miao, L.;Jiang, J.; Gogotsi, Y. MoS_2-on-MXene heterostructures as highly reversible anode materials for lithium-ion batteries. *Angewandte Chemie International Edition* **2018**, *57*, 1846-1850.

[27] Kim, H.;Wang, Z.; Alshareef, H. N. MXetronics: Electronic and photonic applications of MXenes. *Nano Energy* **2019**, *60*, 179-197.

[28] Halim, J.;Lukatskaya, M. R.;Cook, K. M.;Lu, J.;Smith, C. R.;Näslund, L.-Å.;May, S. J.;Hultman, L.;Gogotsi, Y.; Eklund, P. Transparent conductive two-dimensional titanium carbide epitaxial thin films. *Chemistry of Materials* **2014**, *26*, 2374-2381.

[29] Yang, S.;Zhang, P.;Wang, F.;Ricciardulli, A. G.;Lohe, M. R.;Blom, P. W.; Feng, X. Fluoride-free synthesis of two-dimensional titanium carbide (MXene) using a binary aqueous system. *Angewandte Chemie* **2018**, *130*, 15717-15721.

[30] Kim, Y.-J.;Kim, S. J.;Seo, D.;Chae, Y.;Anayee, M.;Lee, Y.;Gogotsi, Y.;Ahn, C. W.; Jung, H.-T. Etching mechanism of monoatomic aluminum layers during MXene synthesis. *Chemistry of Materials* **2021**, *33*, 6346-6355.

[31] Du, Z.;Guo, Y.;Wang, H.;Gu, J.;Zhang, Y.;Cheng, Z.;Li, B.;Li, S.; Yang, S. High-Throughput Production of 1T MoS2 Monolayers Based on Controllable Conversion of Mo-Based MXenes. *ACS nano* **2021**, *15*, 19275.

[32] Sang, X.;Xie, Y.;Lin, M.-W.;Alhabeb, M.;Van Aken, K. L.;Gogotsi, Y.;Kent, P. R.;Xiao, K.; Unocic, R. R. Atomic defects in monolayer titanium carbide (Ti3C2T x) MXene. *ACS nano* **2016**, *10*, 9193-9200.

[33] Pan, W.;Tian, R.;Jin, H.;Guo, Y.;Zhang, L.;Wu, X.;Zhang, L.;Han, Z.;Liu, G.; Li, J. Structure, optical, and catalytic properties of novel hexagonal metastable h-MoO3 nano-and microrods synthesized with modified liquid-phase processes. *Chemistry of Materials* **2010**, *22*, 6202-6208.

[34] Wen, M.;Chen, X.;Zheng, Z.;Deng, S.;Li, Z.;Wang, W.; Chen, H. In-plane anisotropic raman spectroscopy of van der Waals α-MoO3. *The Journal of Physical Chemistry C* **2020**, *125*, 765-773.

[35] de Barros Santos, E.;Sigoli, F. A.; Mazali, I. O. Study of structure of the TiO2–MoO3 bilayer films by Raman spectroscopy. *Materials Research Bulletin* **2014**, *60*, 242-246.

[36] Okeil, S.;Yadav, S.;Bruns, M.;Zintler, A.;Molina-Luna, L.; Schneider, J. J. Photothermal catalytic properties of layered titanium chalcogenide nanomaterials. *Dalton Transactions* **2020**, *49*, 1032-1047.

[37] Huang, X.;Tang, J.;Luo, B.;Knibbe, R.;Lin, T.;Hu, H.;Rana, M.;Hu, Y.;Zhu, X.; Gu, Q. Sandwich-like ultrathin TiS2 nanosheets confined within N, S codoped porous carbon as an effective polysulfide promoter in lithium-sulfur batteries. *Advanced Energy Materials* **2019**, *9*, 1901872.

[38] Choi, K. H.; Suh, D. H. A vacancy-driven phase transition in MoX 2 (X: S, Se and Te) nanoscrolls. *Nanoscale* **2018**, *10*, 7918-7926.

[39] Liu, Z.;Nie, K.;Qu, X.;Li, X.;Li, B.;Yuan, Y.;Chong, S.;Liu, P.;Li, Y.; Yin, Z. General Bottom-Up Colloidal Synthesis of Nano-Monolayer Transition-Metal Dichalcogenides with High 1T′-Phase Purity. *Journal of the American Chemical Society* **2022**.

[40] Nam, G. H.;He, Q.;Wang, X.;Yu, Y.;Chen, J.;Zhang, K.;Yang, Z.;Hu, D.;Lai, Z.; Li, B. In-Plane Anisotropic Properties of 1T′-MoS2 Layers. *Advanced Materials* **2019**, *31*, 1807764.

[41] Acerce, M.;Voiry, D.; Chhowalla, M. Metallic 1T phase MoS 2 nanosheets as supercapacitor electrode materials. *Nature nanotechnology* **2015**, *10*, 313-318.

[42] Liu, Q.;Li, X.;He, Q.;Khalil, A.;Liu, D.;Xiang, T.;Wu, X.; Song, L. Gram-scale aqueous synthesis of stable few-layered 1T-MoS2: applications for visible-light-driven photocatalytic hydrogen evolution. *Small* **2015**, *11*, 5556-5564.

[43] Mendes, R. G.;Ta, H. Q.;Yang, X.;Li, W.;Bachmatiuk, A.;Choi, J. H.;Gemming, T.;Anasori, B.;Lijun, L.; Fu, L. In Situ N-Doped Graphene and Mo Nanoribbon Formation from Mo2Ti2C3 MXene Monolayers. *Small* **2020**, *16*, 1907115.

[44] Ding, W.;Hu, L.;Dai, J.;Tang, X.;Wei, R.;Sheng, Z.;Liang, C.;Shao, D.;Song, W.; Liu, Q. Highly ambient-stable 1T-MoS2 and 1T-WS2 by hydrothermal synthesis under high magnetic fields. *ACS nano* **2019**, *13*, 1694-1702.

[45] Lim, K. R. G.;Handoko, A. D.;Johnson, L. R.;Meng, X.;Lin, M.;Subramanian, G. S.;Anasori, B.;Gogotsi, Y.;Vojvodic, A.; Seh, Z. W. 2h-Mos2 on Mo2ct X Mxene Nanohybrid for Efficient and Durable Electrocatalytic Hydrogen Evolution. *ACS nano* **2020**, *14*, 16140-16155.

[46] Yan, B.;Zhang, B.;Nie, H.;Li, G.;Sun, X.;Wang, Y.;Liu, J.;Shi, B.;Liu, S.; He, J. Broadband 1T-titanium selenide-based saturable absorbers for solid-state bulk lasers. *Nanoscale* **2018**, *10*, 20171-20177.

[47] Lukatskaya, M. R.;Mashtalir, O.;Ren, C. E.;Dall'Agnese, Y.;Rozier, P.;Taberna, P. L.;Naguib, M.;Simon, P.;Barsoum, M. W.; Gogotsi, Y. Cation intercalation and high volumetric capacitance of two-dimensional titanium carbide. *Science* **2013**, *341*, 1502-1505.

[48] Giannozzi, P.;Baroni, S.;Bonini, N.;Calandra, M.;Car, R.;Cavazzoni, C.;Ceresoli, D.;Chiarotti, G. L.;Cococcioni, M.; Dabo, I. QUANTUM ESPRESSO: a modular and open-source software project for quantum simulations of materials. *Journal of physics: Condensed matter* **2009**, *21*, 395502.